Study on the variation mechanism of non-linear stiffness of rubber O-ring

Ting Deng[1], Xunyan Yin[2], Yuqi Yan[3], Hailun Zhou[4], Ran Zhang[5]
[1]AECC Hunan Aviation Powerplant Research Institute, Zhuzhou, 412000, China
[2, 3, 4, 5]School of Aeroengine, Shenyang Aerospace University, Shenyang, 110136, China
[4]Liaoning Key Lab of Advanced Test Technology for Aerospace Propulsion System, Shenyang, 110136, China
[1, 2]Corresponding authors
E-mail: [1]*hnzzdt@qq.com*, [2]*yinxunyan@sau.edu.cn*, [3]*2155053685@qq.com*, [4]*hlzhou@sau.edu.cn*, [5]*2634505164@qq.com*

Received 25 January 2025; accepted 26 June 2025; published online 12 August 2025
DOI https://doi.org/10.21595/jve.2025.24806

Abstract. O-ring dampers can be used as vibration-damping elements for short-life, low-cost engines, and the selection of a suitable rubber superelastic-viscoelastic ontological model to study their stiffness and damping is an important prerequisite for determining their vibration-damping characteristics. The superelastic-viscoelastic constitutive model consists of two models, superelastic and viscoelastic, in which the superelastic model reflects the static characteristics of the O-ring. Therefore, it is the basis of the study of dynamic characteristics to carry out the research on the static stiffness of the O-ring and to select an accurate superelastic model to describe its deformation and recovery characteristics under different working conditions. Based on the fact that the O-ring is in a small deformation range in the damper and the applicability of finite element simulation, the Mooney-Rivilin superelastic constitutive model is selected in this paper. Establish a three-dimensional finite element model of the O-ring damper, focusing on the analysis of the effect of temperature on the O-ring material properties and damper structure, to reveal the mechanism of non-linear stiffness change of the O-ring damper. At the same time, the accuracy of the hyperelastic model is verified by the test method, which lays a foundation for the study of the dynamic stiffness and damping characteristics of the O-ring. The results show that in the pre-compression state, there is a large contact pressure between the O-ring and the inner and outer rings of the damper. The contact pressure increases linearly during the compression process, and the stiffness of the O-ring changes linearly. In the non-pre-compression state, the contact pressure is 0, the contact pressure increases nonlinearly during the compression process, and the stiffness of the O-ring shows obvious nonlinear characteristics. In addition, the static stiffness of the O-ring increases with the increase of pre-compression amount, increases with the increase of material hardness, and decreases with the increase of temperature. The above research provides a reference for selecting the appropriate O-ring material size and installation conditions in the project to ensure that the O-ring can effectively withstand pressure during use.

Keywords: O-ring damper, nonlinear stiffness, contact pressure, numerical simulation.

Nomenclature

Notation	Description
W	Potential energy of strain
λ_1	Main stretch ratio in the x direction
λ_2	Main stretch ratio in the y direction
λ_3	Main stretch ratio in the z direction
C_{ij}	Rubber material parameters
D_i	Material constant
I_1	First-order strain invariants
I_2	Second-order strain invariants

I_3	Third-order strain invariants
J	Volume ratio
l_i	The original length in the direction of the main axis
Δl_i	The length increment in the direction of the main axis
C_{10}	Rubber material parameters
C_{01}	Rubber material parameters
G	Shear modulus
E	Elastic modulus
H_r	Hardness
ΔF	The load difference between two neighboring measurement points
ΔX	The displacement difference.
K_r	Stiffness

1. Introduction

Short-lifespan, low-cost engines are commonly used in strategic missiles. These engines have a very short lifespan, thus requiring them to be simple to manufacture, low in cost, and highly efficient. Dampers, as important vibration reduction components of the engine rotor system, must also possess characteristics such as simplicity in manufacturing and low cost, consistent with the engine's requirements. O-ring dampers utilize rubber O-rings as the damping elements, which dissipate energy through the viscoelastic damping of rubber under vibrational displacement, providing effective vibration reduction. They offer advantages such as compact structure, ease of use, simple manufacturing, low cost, and no pollution. Therefore, applying O-ring dampers to this type of engine can not only achieve a good vibration reduction effect but also reduce the overall cost of the engine, demonstrating promising development prospects and economic benefits.

As a vibration-damping element, the stiffness characteristic of rubber material is one of the important parameters for evaluating the vibration-damping performance, which has received extensive attention from scholars at home and abroad [1-12]. Selecting an appropriate hyperelastic constitutive model for rubber is a prerequisite for investigating stiffness characteristics. Zhang [13] established finite element models for uniaxial compression tests of silicone rubber, nitrile rubber, and fluor rubber based on the Mooney-Rivlin (M-R) and Yeoh models. The nominal stress-strain curves and simulations of these three rubber materials were compared. The results demonstrated that the M-R model is suitable for small deformation behaviors of rubber, while the Yeoh model better describes large deformation behaviors. Li [14], addressing the tendency of the Yeoh model to underpredict stiffness, proposed a modified Yeoh hyperelastic constitutive model based on the large deformation theory of continuum mechanics. The results indicated that the Yeoh model can accurately predict stress-strain relationships under uniaxial, planar, and equibiaxial tension-compression across a wide strain range. As evidenced by these studies, the M-R model provides more accurate descriptions of the static characteristics of O-rings due to the small deformation features of O-ring dampers.

The determination of M-R model parameters currently relies on two primary methods: experimental testing and empirical formulas. Zheng [15] employed nonlinear finite element analysis and axial compression tests to determine the mechanical property constants C_1 and C_2 of rubber materials for the M-R model. Wang [16] investigated the relationship between the stiffness and hardness of rubber components. By leveraging rubber hardness experimental data, he established an exponential quadratic nonlinear function linking hardness to M-R model parameters, thereby converting the relationship between elastic modulus and hardness into one between elastic modulus and material parameters C_1 and C_2. Luo [17] studied the performance of rubber vibration isolation bearings in marine corrosion environments, determining M-R model parameters via empirical formulas and observing linear variations in bearing stiffness.

In summary, both experimental testing and empirical formulas can yield hyperelastic model parameters. However, for systematic investigation of the influence of O-ring hardness on its

mechanical properties, empirical formulas offer greater convenience for determining M-R model parameters. To validate the accuracy of this approach, this paper proposes static stiffness tests to measure the static stiffness of O-rings.

Domestic research on the stiffness and damping characteristics of rubber O-rings commenced relatively early. In 1987, Yin [18] experimentally measured the stiffness coefficients of O-rings supporting gas bearings, focusing on the effects of rubber material, supply pressure, and installation compression on stiffness. Qi et al. [19] employed the Mooney-Rivlin model to simulate the stiffness of rubber elastic wheels via finite element analysis, investigating the influence of wheel structure and press-fitting on stiffness characteristics. Chen [20] conducted experimental and numerical studies on the static stiffness of rubber vibration isolation rings, examining the effects of ring structure and rubber material hardness on stiffness. Horton et al. [21, 22] calculated the stiffness of rubber bushings using a nonlinear shape factor method. Lin [23] analyzed the temperature characteristics of rubber standard blocks and obtained correction coefficients for hardness values at different temperatures. Elshabrawy et al. [24-28] proposed a computational model to predict the nonlinear behavior of rubber materials. As evidenced by these studies, research on rubber material stiffness has primarily focused on material hardness and vibration isolation structure impacts. Rubber stiffness often exhibits linear variations in these works, failing to capture its nonlinear characteristics, while the underlying mechanisms driving this linear behavior remain unclear. Additionally, although high temperatures during engine operation necessitate consideration of thermal effects on O-ring stiffness, existing studies have not accounted for temperature influences, leaving the investigation of rubber material stiffness characteristics incomplete.

Therefore, it is necessary to carry out a systematic study on the stiffness characteristics of O-ring dampers, including the static stiffness and dynamic stiffness of O-ring dampers. The static stiffness is used to evaluate the static performance of the O-ring damper, based on the hyperelasticity principal model of the rubber material; the dynamic stiffness is used to evaluate the dynamic performance of the O-ring damper, based on the hyperelasticity-viscoelasticity principal model of the rubber material. Therefore, the selection of a suitable hyperelastic principal model to accurately describe the static properties of O-rings is the basis for carrying out the study of their dynamic properties, which has a crucial impact on the vibration damping performance of O-ring dampers.

In summary, this study focuses on investigating the static characteristics of O-rings. First, the Mooney-Rivlin (M-R) hyperelastic constitutive model for rubber materials is established. Model parameters are determined using two approaches – uniaxial tensile tests and empirical formulas – with the stiffness results from both methods compared to define the criteria for hyperelastic model parameter selection. Based on this, finite element simulations of O-ring stiffness are conducted, and experimental tests are employed to validate the accuracy of the hyperelastic constitutive model. Finally, the effects of temperature, installation interference, and material hardness on O-ring stiffness are analyzed. Special attention is given to the thermal deformation of the damper's inner and outer rings under engine operating temperatures. By coupling the pre-compression and hardness of O-rings, the variation mechanism of nonlinear stiffness in O-ring dampers is revealed.

Through this research, a deeper understanding of the deformation and recovery characteristics of O-rings under various working conditions is achieved, guiding the selection of appropriate O-ring materials and dimensions in engineering design to ensure effective pressure-bearing performance during service. In subsequent studies on the vibration damping characteristics of O-ring dampers, the hyperelastic model developed here will be combined with a viscoelastic model to investigate dynamic stiffness and damping properties. Therefore, the investigation of O-ring damper static characteristics is essential, as it serves as the foundation for dynamic characteristic research.

2. Finite element calculation of static stiffness

2.1. Hyperelasticity principal model theory

Rubber is a hyperelastic approximately incompressible material, and the intrinsic relationship of rubber materials can be described according to the strain energy function based on the image-only theory. The image-only theory assumes that rubber is isotropic in the undeformed state as well as during deformation. Mooney [13, 17] derived the strain energy function based on the image-only theory of large elastic deformation as:

$$W = C_1(\lambda_1^2 + \lambda_2^2 + \lambda_3^2 - 3) + C_2(\lambda_1^{-2} + \lambda_2^{-2} + \lambda_3^{-2}), \tag{1}$$

where, λ_1, λ_2, λ_3 is the main stretch ratio in all three directions.

Rivlin [13, 17] introduced strain invariants into the strain energy function. Based on the above assumptions, the strain energy function is considered to be symmetric with respect to the three principal stretch ratios, i.e., changing the sign of the principal stretch ratios has no effect on the strain energy function. In order to satisfy the boundary condition that the strain energy is zero at zero strain ($\lambda_1 = \lambda_2 = \lambda_3 = 1$), the strain energy function is given as:

$$W = \sum_{i+j=1}^{N} C_{ij}\,(I_1 - 3)^i (I_2 - 3)^j + \sum_{i=1}^{N} 1/D_i (J-1)^{2i}, \tag{2}$$

$$I_1 = \lambda_1^2 + \lambda_2^2 + \lambda_3^2, \tag{3}$$

$$I_2 = \lambda_1^2\lambda_2^2 + \lambda_2^2\lambda_3^2 + \lambda_1^2\lambda_3^2, \tag{4}$$

$$I_3 = \lambda_1^2\lambda_2^2\lambda_3^2, \tag{5}$$

$$\lambda_i = \frac{l_i + \Delta l_i}{l_i}, \quad (i = 1,2,3), \tag{6}$$

where, I_1, I_2, I_3, are first-, second-, and third-order strain invariants; D_i is a material constant; J is volume ratio; l_i is the original length in the direction of the main axis; Δl_i is the length increment in the direction of the main axis. Due to the incompressibility of rubber, $\lambda_1^2\lambda_2^2\lambda_3^2 = 1$.

Based on the intrinsic model of rubber derived by Rivlin, various other forms of strain energy functions have been developed. There are Mooney-Rivlin model, Yeoh model, Neo-Hookean model, etc.; for general rubber materials, Mooney-Rivlin model can more accurately describe the performance of rubber materials with deformation less than 150 % [19], and is suitable for finite element analysis. Therefore, the Mooney-Rivlin model is chosen to simulate the superelastic characteristics of O-rings, and the first two items are expanded by taking $N = 1$ on the basis of the Rivlin model, i.e., it is the Mooney-Rivlin model, and its strain energy function is:

$$W = C_{10}(I_1 - 3) + C_{01}(I_2 - 3) + \frac{1}{D_1(J-1)^2}, \tag{7}$$

where, C_{10} and C_{01} are rubber material parameters.

For incompressible rubber materials (Poisson's ratio $\upsilon \approx 0.5$), the shear modulus G is related to the elastic modulus E at small strains as follows:

$$G = \frac{E}{2(1+\upsilon)}. \tag{8}$$

When Poisson's ratio υ is approximately taken as 0.5, it can be obtained that $E = 3G$, and at the same time $G = 2(C_{10} + C_{01})$, it can be obtained that the elastic modulus of the rubber material has the following relationship with the material parameters:

$$E = 6C_{10}\left(1 + \frac{C_{01}}{C_{10}}\right). \tag{9}$$

In literature [15], the relationship between IRHD hardness, H_r, and elastic modulus, E, was fitted from experimental data as:

$$\lg E = 0.0198H_r - 0.5432. \tag{10}$$

According to literature [17], when $C_{01}/C_{10} = 0.25$ and the hardness of the O-ring is 70 A, $C_{10} = 0.9284$ MPa and $C_{01} = 0.2321$ MPa are obtained.

2.2. O-ring damper structure

In this paper, the O-ring damper structure used to match an engine, damper inner and outer ring between the arrangement of 2 rings O-ring (due to the symmetry of the 2-ring O-ring structure, in the schematic diagram only indicates a single O-ring) local structure schematic shown in Fig. 1. Among them, the O-ring material is fluorine rubber, the inner and outer sides of the O-ring are the inner and outer rings of the damper, the material of the inner and outer rings is structural steel, and the part of the geometric model that overlaps is the O-ring's excess. The parameters of the structural part of the damper are shown in Table 1.

2.3. O-ring static stiffness finite element analysis

2.3.1. Modeling and meshing

In this paper, the finite element software Ansys is used to simulate the static characteristics of the O-ring damper, and its three-dimensional model is shown in Fig. 2. In order to improve the calculation speed, the inner and outer rings of the damper are simplified. The bearing and elastic support are simplified as the inner ring, the magazine is simplified as the outer ring, two symmetrically positioned O-rings are mounted on the grooves of the inner ring, and the oil supply holes and rounded corners, Ignore the oil supply holes and rounded corners which have less effect on stiffness, which have a small influence on the stiffness, are ignored. In order to avoid the deformation of the inner and outer rings having a large impact on the stiffness of the O-ring, the modulus of elasticity of the inner and outer rings is much larger than that of the O-ring, which is treated as a rigid body.

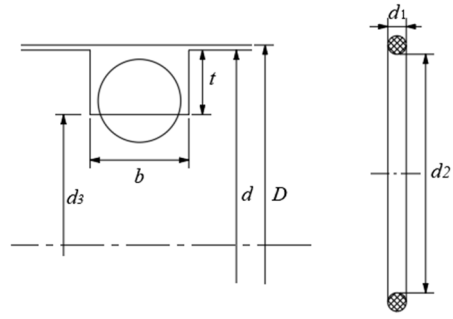

Fig. 1. Structure diagram of O-ring damper

Table 1. Structural parameters of O-ring damper

Inner ring outer diameter d	Inner diameter of outer ring D	Bottom diameter of groove D_3	Groove depth T	Groove width b	Inner diameter of O-ring d_2	O-ring cross-sectional diameter d_1
75	75.22	72.2	1.4	2.15	71	1.8

To facilitate meshing and ensure mesh quality, the O-ring is split from the inner ring of the damper. The cell type is selected as 186 cells. The mesh is made of hexahedral cells, and the mesh is encrypted for the cross section of the O-ring. After the mesh-independence verification, the static stiffness of the O-ring tends to be stabilized when the circumferential mesh size of the O-ring is 0.5 mm and the cross-section mesh size is 0.2 mm. Considering the computational accuracy as well as the computational resources, the circumferential mesh of the O-ring is selected to be 0.5 mm, and the cross-section mesh to be 0.2 mm.

2.3.2. Contact setup

There is contact between the O-ring and the inner surface of the outer ring and the groove. As the outer ring squeezes the rubber O-ring to different degrees, the area of the contact surface between the O-ring and the outer ring and the groove changes all the time, and there is a high degree of non-linearity in this contact. Applying the three-dimensional surface contact units CONTA174 and TRAGE170 to establish contact pairs at the O-ring and the inner and outer rings, the surface of the O-ring is used as the contact surface, and the surface in contact with it is used as the target surface. There is permeability between the contact pairs, and the smaller the permeability tolerance is, the higher the computational accuracy is, and at the same time, the more difficult it is to converge. Considering the computational accuracy of the model and the convergence problem, the contact algorithm adopts the augmented Lagrangian method, and the permeability tolerance is taken as 0.01 mm.

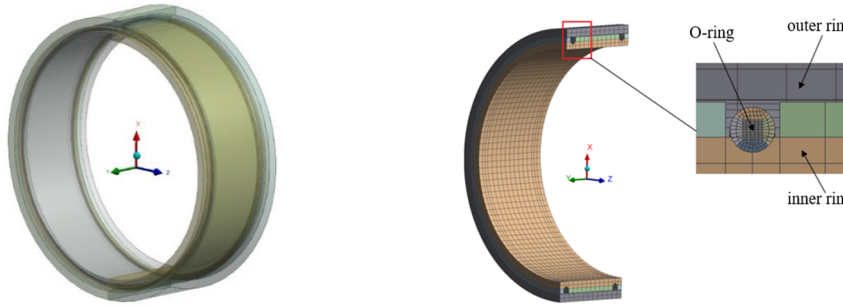

a) Finite element modeling b) Schematic diagram of gridding

Fig. 2. Three-dimensional model of O-ring damper

2.3.3. Boundary conditions and numerical solution

According to the assembly and loading process of the O-ring, the loading step is divided into two steps, as shown in Fig. 3.

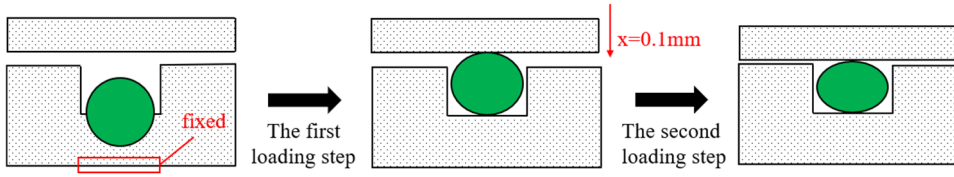

Fig. 3. Assembly and loading process of the O-ring

In the first step, a geometric modeling of interference is used to simulate the interference assembly of the O-ring with the inner ring. The surface of the inner ring of the damper is fixedly supported, and the sides of the outer ring are free in the radial direction, constraining the freedom in the remaining two directions. In the second step, the extrusion process of the outer ring on the O-ring is simulated. In order to prevent the force applied to the outer ring from being too large to

ISSN PRINT 1392-8716, ISSN ONLINE 2538-8460

cause the inner and outer rings to collide, which would cause the stiffness to vary greatly, the displacement load is used instead of the force load. Considering that the actual gap between the inner and outer rings is 0.11 mm, a displacement load of 0.1 mm linearly increasing along the x-direction is applied to the outer surface of the outer ring.

2.3.4. Analysis of numerical simulation results

The displacement cloud of the O-ring damper after the interference assembly as well as the compression process is shown in Fig. 4. The inner ring of the damper is fixed during assembly, and the radial reaction force on the outer ring when the O-ring is recovered from interference is uniformly distributed and counteracts each other, so that the inner and outer rings do not move and the radial reaction force on the outer ring is zero. When the outer ring is compressed in the x-direction, one end of the O-ring is squeezed and one end is released slowly, the radial reaction force on the outer ring at the squeezed end increases, and the radial reaction force on the outer ring at the released end decreases, so that the outer ring is subjected to an increase in the total radial reaction force along the x-direction.

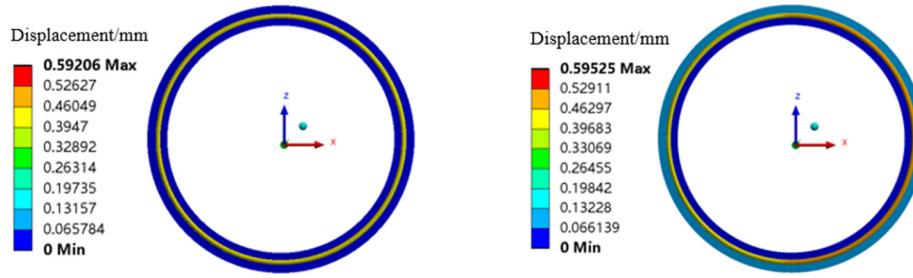

a) Displacement cloud after interference assembly b) Compressed displacement cloud

Fig. 4. Displacement cloud diagram of O-ring damper

The radial reaction force of the O-ring on the outer ring during the extrusion process is calculated, and the difference between the neighboring loads and displacements is used to calculate the static stiffness of the O-ring in this system, and the results are shown in Fig. 5.

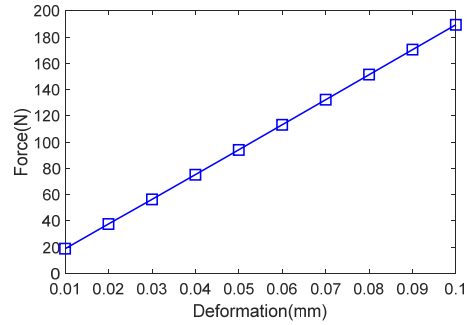

Fig. 5. Stiffness characteristics of the O-ring under 0.29 mm compression

The stiffness equations are as follows:

$$K_r = \frac{\Delta F}{\Delta X}, \tag{11}$$

where $\Delta F$is the load difference between two neighboring measurement points; ΔX is the displacement difference.

The results show that although the rubber material is a nonlinear material, the static load of the

O-ring shows an approximately linear relationship with the change of displacement, and the stiffness magnitude is 1.8939×10^6 N/m. This is because the maximum gap between the inner and outer rings of the damper is only 0.11 mm, each time the displacement of the O-ring increases in 0.01 mm or so, until its displacement reaches 0.1 mm; and the interference fit leads to the O-ring in the initial moment there has been 0.29 mm of pre-compression, pre-compression makes the O-ring and the inner and outer rings of the damper between the contact pressure is greater. Therefore, the stiffness results show an approximately linear relationship.

3. Static stiffness test

In order to successfully carry out the subsequent research on the dynamic characteristics of the O-ring damper and to verify the accuracy of the Mooney-Rivlin superelastic intrinsic model, the static stiffness characteristics of the O-ring were experimentally tested.

3.1. Test program

In order to study the stiffness characteristics of O-rings, a static stiffness test rig for O-rings was designed and constructed, as shown in Fig. 6, and the main test equipment included: O-ring, force transducer, displacement transducer, damper inner and outer rings, etc. In this case, the squirrel cage elastic support is used as the damper outer ring, and the shaft as the inner ring. O-ring static stiffness determination is to simulate its working force in non-working condition. In the operating condition, the vibration of the journal is transmitted to the inner surface of the inner ring and the actual load is applied to the inner ring. During the test, in order to facilitate the test, a horizontal tension force is applied to the outer ring of the O-ring damper, and a displacement sensor is set up on the opposite side of the tension direction. After applying the force to the O-ring, its deformation under different static loads is measured, so as to determine its stiffness characteristics.

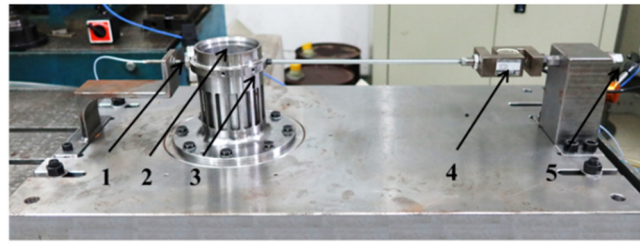

1.displacement transducer 2.inner ring 3.outer ring 4.force transducer 5.loading device

Fig. 6. O-ring static stiffness test-bed

3.2. Analysis of test results

The O-ring static stiffness test results and simulation calculations are shown in Fig. 7. The overall trend of the simulation and experimental curves is consistent, and the experimental test static stiffness magnitude is 1.799×10^6 N/m. The error between the simulated and tested values is within 5.27 %. This proves the accuracy of the selection of the O-ring superelastic intrinsic model and the rationality of the finite element modeling method. The error between the simulation and the test comes from the assembly of the test piece and the machining error that makes the gap between the inner and outer rings deviate from the actual value.

4. Analysis of factors affecting the static stiffness of O-rings

In the actual assembly, the interference fit makes the O-ring acquire a certain amount of

pre-compression, resulting in a sufficiently large contact pressure between the O-ring and the inner and outer rings of the damper, while the maximum displacement deformation of the test loading is only 0.1 mm, so the stiffness characteristics of the O-ring varies linearly in the above tests and simulations. In order to eliminate the limitation of the test structure, the static stiffness of the O-ring will continue to be simulated using the Mooney-Rivlin model in this section to obtain the nonlinear characteristics of the O-ring stiffness.

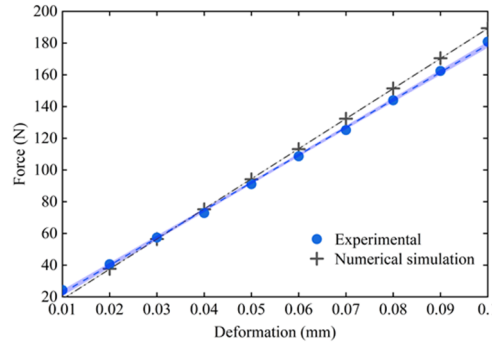

Fig. 7. Comparison of O-ring stiffness test and simulation under 0.29 mm compression

4.1. Effect of precompression on static stiffness of O-rings

During engine operation, the proper amount of pre-compression will provide sufficient contact pressure between the O-ring and the inner and outer rings to realize the sealing effect while providing sufficient support stiffness. In this section, the effect of pre-compression on the static stiffness of O-rings is investigated by adjusting the outer ring size to change the amount of O-ring pre-compression. The relationship between the outer ring size and the amount of pre-compression is shown in Table 2.

Table 2. Relationship between outer ring size and pre-compression amount

Inner diameter of outer ring (mm)	75.22	75.32	75.42	75.8
pre-compression (mm)	0.29	0.24	0.19	0

The contact state of the O-ring without pre-compression is illustrated in Fig. 8(a). In this scenario, the cross-sectional diameter d_1 of the O-ring equals the distance e_1 from the groove bottom to the outer ring ($d_1 = e_1$). After assembly, no contact pressure exists between the damper's outer ring and the O-ring. Fig. 8(b). depicts the contact state under pre-compression. Here, the O-ring's cross-sectional diameter d_1 exceeds the distance e_1 from the groove bottom to the outer ring ($d_1 > e_1$). Following interference assembly, contact pressure develops between the outer ring and the O-ring, with both the contact width and pressure increasing as the outer ring compresses the O-ring.

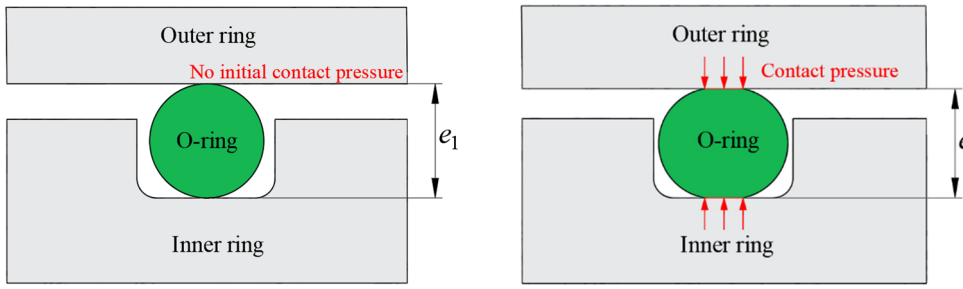

a) O-ring contact state without pre-compression b) O-ring contact state with pre-compression

Fig. 8. Contact state between the O-ring and the outer ring of the damper with and without pre-compression

Fig. 9. shows the stiffness characteristics of the O-ring under different pre-compressions. From the stiffness change rule, in the pre-compression state, the O-ring stiffness curve basically maintains the linearity; while in the state without pre-compression, the O-ring stiffness increases continuously with the displacement increase, and shows obvious non-linear characteristics.

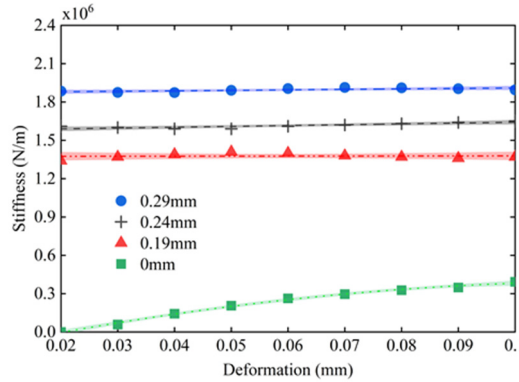

Fig. 9. The variation curve of O-ring stiffness with displacement under different pre-compressions

In order to analyze this phenomenon, the contact pressure (hereinafter referred to as "contact pressure") of the entire O-ring before the start of loading with and without pre-compression was calculated, and the results are shown in Fig. 10. It can be found that when there is pre-compression (interference fit), contact pressure is generated where the O-ring contacts the inner and outer rings, and the maximum contact pressure is located at the centre of the contacting segment and decreases gradually to both sides, while when the pre-compression is 0 (no interference fit), there is no contact pressure. As the displacement of the O-ring increases, its contact pressure with the inner and outer rings increases, as shown in Fig. 11.

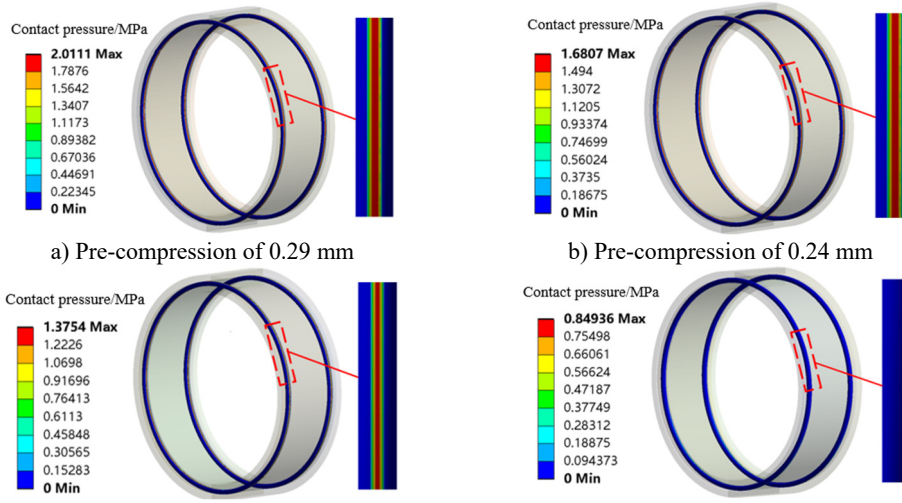

a) Pre-compression of 0.29 mm

b) Pre-compression of 0.24 mm

c) Pre-compression of 0.19 mm

d) Pre-compression of 0 mm

Fig. 10. Initial contact pressure of the O-ring under different pre-compressions

Combining Fig. 10. and Fig. 11, it can be found that when there is precompression of the O-ring, the contact pressure increases linearly with the increase of displacement. 0.29 mm of precompression, the initial maximum contact pressure is 2.01 MPa, and when the displacement of the O-ring is increased by 0.01 mm, the contact pressure is only increased by about 0.1 MPa; when the displacement of the O-ring is increased to a maximum of 0.1 mm, the contact pressure is

ISSN PRINT 1392-8716, ISSN ONLINE 2538-8460

increased by a total of about 0.7 MPa. For the 0.24 mm and 0.19 mm pre-compressed states, similar results also occur. This indicates that the increase in contact pressure during compression of the O-ring is much smaller than the initial contact pressure, while the contact pressure increases linearly, and both of them together make the O-ring unable to show nonlinear characteristics. While the initial contact pressure is 0 when the O-ring is not pre-compressed, the contact pressure increases by a total of about 0.9 MPa as the displacement increases to 0.1 mm, and at the same time, the contact pressure increases nonlinearly with the increase of displacement, so that the O-ring exhibits an obvious nonlinear characteristic. In addition, the contact pressure increases as the amount of pre-compression increases, so the stiffness of the O-ring increases as the amount of pre-compression increases.

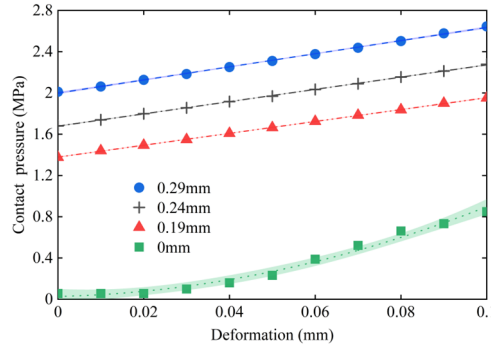

Fig. 11. The contact pressure of O-ring changes with displacement under different pre-compression

4.2. Effect of hardness on static stiffness of O-rings

Fluoroelastomers are highly stable and can withstand high temperatures, oil media, and a wide range of chemicals. And for the same fluoroelastomer material with different hardness, its material properties will be different. Keeping the structural dimensions of the O-rings unchanged, the static stiffness characteristics under the hardnesses of 65 A, 70 A, 75 A, 80 A, and 85 A were examined respectively, the hardness of the rubber material was changed, and the corresponding parameter values of the M-R model could be obtained according to Eq. (9) and Eq. (10), and the other constraints and loading conditions remained unchanged.

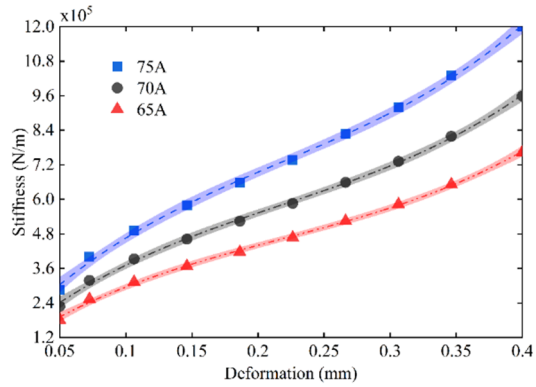

Fig. 12. Changes of stiffness of three kinds of hardness O-rings with displacement without pre-compression

The simulation results for the influence of O-ring hardness on static stiffness under no pre-compression are shown in Fig. 12. As illustrated, the static stiffness of the O-ring increases with higher hardness under no pre-compression. This is attributed to the increased elastic modulus

of the rubber material at greater hardness, which enhances its resistance to deformation, thereby elevating stiffness. Additionally, all three hardness levels of O-rings exhibit pronounced nonlinear characteristics in the absence of pre-compression.

Fig. 13. shows the curve of O-ring stiffness versus hardness with precompression. Similar to the case without pre-compression, the stiffness of the O-ring with pre-compression also increases with the increase of O-ring hardness. At 0.29 mm pre-compression, the hardness change from 65 A to 85 A increased the stiffness by 2.24×10^6 N/m. At 0.24 mm pre-compression, the stiffness increases by 1.91×10^6 N/m. The stiffness increased by 1.63×10^6 N/m at 0.19 mm of pre-compression. This means that the higher the pre-compression, the more the O-ring stiffness is affected by the hardness.

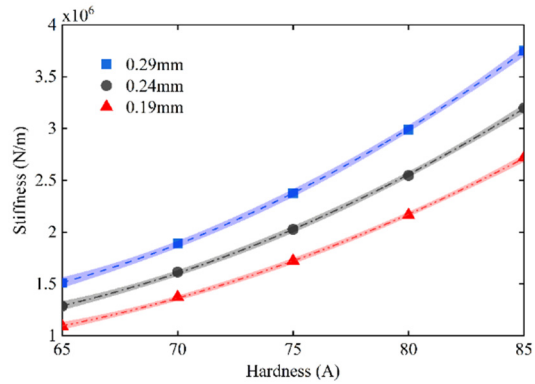

Fig. 13. The variation curve of O-ring stiffness with hardness during pre-compression

4.3. Effect of temperature on static stiffness of O-rings

During engine operation, its temperature changes constantly, causing the temperature of the O-ring damper to change as well. Temperature changes will cause thermal deformation of the inner and outer rings of the damper, and at the same time, change the hardness of the O-ring. The rubber material properties are related to temperature as follows:

$$H_{rt} = H_{rst} + \beta(T - 23), \tag{12}$$

where H_{rt} is the hardness of the material at ambient temperature T; H_{rst} is the hardness of the material at standard room temperature; T is the ambient temperature; β is the temperature correction coefficient, and $\beta = -0.13$ is taken in the range of 70 A-75 A [23]. An increase in temperature leads to a decrease in the hardness of O-rings. The relationship between rubber hardness and temperature is described by Eq. (12). Based on the correlation between rubber hardness and elastic modulus in Eq. (10), the material parameters of O-rings under varying temperatures are derived and summarized in Table 3.

Table 3. Effect of temperature on O-Ring material parameters

T (°C)	H_r (A)	E (MPa)	C_{10} (MPa)	C_{01} (MPa)
50	66.5	5.94	0.7915	0.1979
100	60	4.41	0.5885	0.1471
150	53.5	3.28	0.4376	0.1094
200	47	2.44	0.3253	0.0813

First, excluding the effect of temperature on the inner and outer rings of the damper, only the effect of temperature on the O-ring must be considered. Fig. 14. shows the results of the effect of operating temperature on the static stiffness of O-rings without pre-compression. From the fig, it can be seen that the static stiffness of the O-ring decreases with the increase in temperature, which

is due to the decrease in the hardness of the O-ring caused by the increase in temperature [23], and the modulus of elasticity decreases, and the ability of the O-ring to resist deformation is reduced, thus the stiffness decreases. In addition, the stiffness of O-rings at different operating temperatures without pre-compression shows obvious non-linear characteristics.

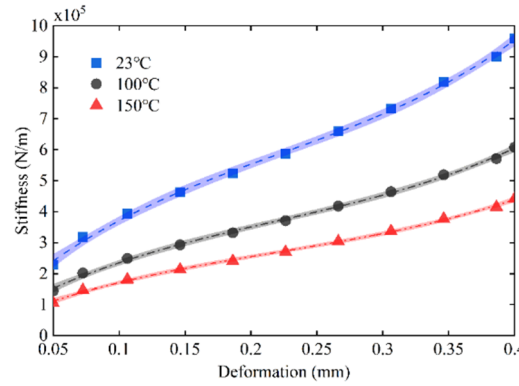

Fig. 14. The change of stiffness of O-ring with displacement at three temperatures without pre-compression

Fig. 15. shows the variation curve of O-ring stiffness with temperature during pre-compression. Similar to the case without pre-compression, the stiffness of O-rings with pre-compression similarly decreased with increasing temperature. The stiffness decreased by 1.23×10^6 N/m for 0.29 mm of pre-compression, 1.05×10^6 N/m for 0.24 mm of pre-compression, and 0.89×10^6N/m for 0.19mm of pre-compression for the range of temperature change from 23 ℃ to 200 ℃. It shows that the O-ring stiffness is more affected by temperature at higher pre-compression.

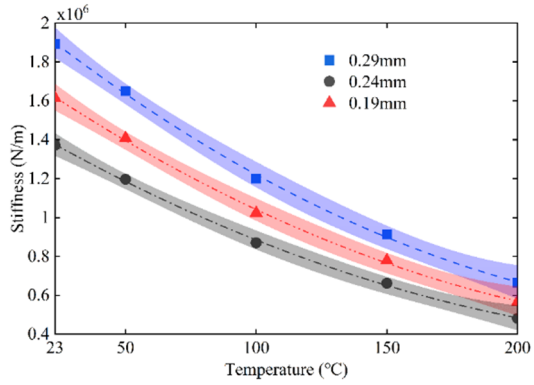

Fig. 15. The change curve of O-ring stiffness with temperature during pre-compression

Secondly, the thermal deformation effects of the damper's inner and outer rings under temperature variations are further considered. As temperature increases, the inner ring expands outward, enlarging the diameter of the groove base. In this study, the referenced engine structure features a fixed outer ring (structural schematic in Fig. 16(a)), where the outer ring contracts inward due to thermal expansion, reducing the squeeze clearance c, thereby increasing the pre-compression and contact pressure. For comparative analysis, the scenario of a freely expanding outer ring surface is also examined (structural schematic in Fig. 16(b)), where outward thermal expansion of the outer ring enlarges the squeeze clearance c, leading to reduced pre-compression and contact pressure. The clearance variations of the damper under different temperatures are listed in Table 4, where $c_1 = 0.11$ mm, represents the initial clearance before deformation, and c_2 denotes the post-deformation clearance.

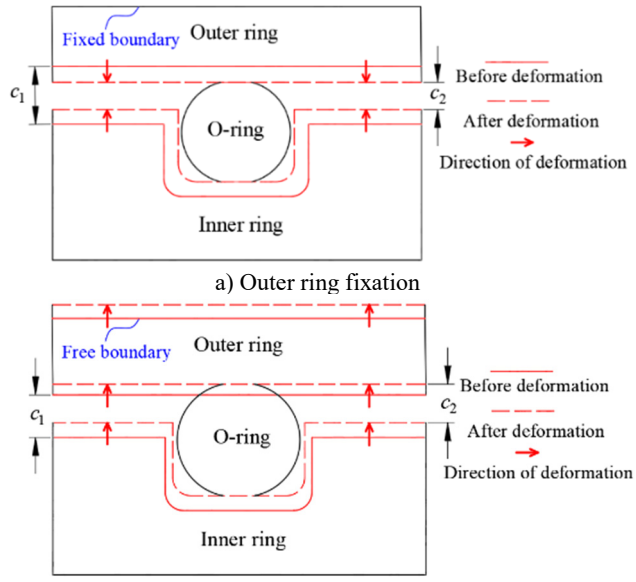

a) Outer ring fixation

b) Outer ring freedom

Fig. 16. Effect of temperature on damper structure at different

Table 4. Effect of temperature on damper gap

T (°C)	c_2 (mm)	
	Fixed boundary	Free boundary
50	0.107	0.122
100	0.102	0.144
150	0.097	0.164
200	0.092	0.188

After coupling the thermal deformation of the inner and outer rings of the damper with the change in the hardness of the O-ring, the effect of temperature on the static stiffness of the O-ring under pre compression of 0.29 mm is shown in Fig. 17.

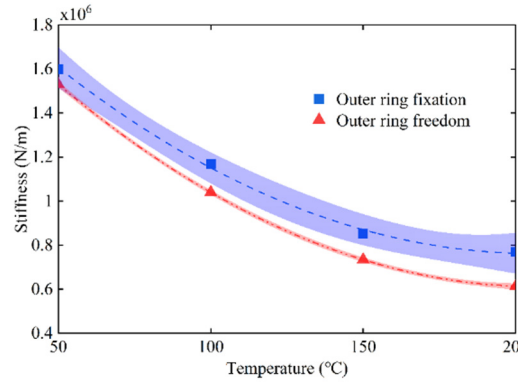

Fig. 17. Variation curve of static stiffness of O-ring with temperature considering deformation of inner and outer rings

In both cases, the static stiffness of the O-ring gradually decreases with the increase of temperature and the trend of change gradually slows down. The higher the temperature, the smaller the effect of temperature on the static stiffness of the O-ring. When the outer ring is fixed, the gap is smaller than when the outer ring is free, and the contact pressure is greater, so the static stiffness

ISSN PRINT 1392-8716, ISSN ONLINE 2538-8460

of the O-ring is greater. And as the temperature increases, the difference in static stiffness between the two cases increases from 4.4 % to 20.4 %.

5. Conclusions

This paper takes the O-ring damper as the research object, uses the numerical simulation method to study the static stiffness characteristics of the rubber O-ring, and analyzes the influence law of different factors on the static stiffness of the O-ring, especially couples the thermal deformation of the inner and outer rings of the damper and the hardness change of the O-ring, and examines the influence of temperature on the static stiffness of the O-ring; at the same time, the experimental test is used to verify the accuracy of superelasticity intrinsic model, and lays the foundation of the study of the O-ring's dynamic At the same time, experimental tests are used to verify the accuracy of the superelastic constitutive model, which lays the foundation for the study of O-ring dynamic stiffness and damping characteristics, and is of guiding significance for the selection and installation of O-rings as well as the design of damper structure. The results of the study are as follows:

1) The static stiffness and contact pressure of O-rings increase with the increase of pre-compression. The static stiffness and contact pressure of O-rings show nonlinear changes at a pre-compression amount lower than 0.19 mm; at a pre-compression amount higher than 0.19 mm, the stiffness and contact pressure of O-rings show linear changes. In order to eliminate the effect of uncertainty brought about by the nonlinear stiffness of the O-ring, it should be ensured that the pre-compression of the O-ring is more than 0.19 mm, and at the same time, the pre-compression should not be too large, so as to avoid that the O-ring arrives at the service life prematurely.

2) The static stiffness of the O-ring increases with the increase in the hardness of the rubber material. And the greater the amount of pre-compression, O-ring stiffness is affected by the hardness of the greater. In the case of ensuring a suitable amount of pre-compression so that the O-ring stiffness linear change, can choose to adjust the hardness of the material to adjust the static stiffness of the O-ring.

3) The static stiffness of the O-ring decreases with the increase of temperature, and the trend of decrease is slowing down, indicating that the higher the temperature, the effect of temperature on stiffness decreases. The larger the amount of pre-compression, the greater the effect of temperature on the static stiffness.

4) Under the consideration of the effect of temperature on the deformation of the inner and outer rings, when the outer surface of the outer ring is fixed, the temperature increase will make the extrusion gap of the O-ring smaller and the static stiffness of the O-ring increase; when the outer surface of the outer ring is free, the temperature increase will make the extrusion gap of the O-ring larger and the static stiffness of the O-ring decrease. The higher the temperature, the more pronounced the difference between the two. Constraining the outer surface of the outer ring will have a compensating effect on the static stiffness of the O-ring.

The research in this paper proves that the Mooney-Rivlin model can accurately describe the superelastic properties of O-rings, laying a foundation for the subsequent establishment of superelastic-viscoelastic models and dynamic characteristic research. In practical applications, on the one hand, O-rings with high hardness, large cross-sectional dimensions, and high temperature resistance can be selected; on the other hand, when designing the damper structure, the depth of the damper groove can be reduced to increase the compression of the O-ring, thereby improving the vibration damping performance of the O-ring damper.

Acknowledgements

The authors have not disclosed any funding.

Data availability

The datasets generated during and/or analyzed during the current study are available from the corresponding author on reasonable request.

Author contributions

Ting Deng: formal analysis and methodology. Xunyan Yin and Hailun Zhou: conceptualization, funding acquisition, and writing review. Yuqi Yan: writing the original draft preparation, investigation, and software. Ran Zhang: visualization and software.

Conflict of interest

The authors declare that they have no conflict of interest.

References

[1] Y. Hou, Y. Sun, and L. M. Hei, "Study on the eccentricity and attitude angle of journal gas bearing with rubber rings support," (in Chinese), *Lubrication Engineering*, Vol. 2, No. 4, pp. 14–16, 2005, https://doi.org/10.3969/j.issn.0254-0150.2005.02.005

[2] H. J. Xuan and W. R. Hong., "Application of elastomer O-rings damper in high speed spin tester," (in Chinese), *Journal of Zhejiang University: Engineering Science*, Vol. 39, No. 12, pp. 1854–1857, 2005, https://doi.org/10.3785/1008-973x.2005.12.1854

[3] J. Wu, "Computational method for dynamic properties of rubber isolators using hyperelastic-viscoelastic-plastoelastic constitutive model," (in Chinese), *Journal of Mechanical Engineering*, Vol. 46, No. 14, p. 109, Jan. 2010, https://doi.org/10.3901/jme.2010.14.109

[4] D. B. Han and X. G. Song, "Experimental study on constitutive model for damping and stiffness of a rubber isolator," (in Chinese), *Journal of Vibration and Shock*, Vol. 28, No. 1, pp. 156–160, 2009, https://doi.org/10.3969/j.issn.1000-3835.2009.01.036

[5] P. Bättig and J. Schiffmann, "Data-driven model for the dynamic characteristics of O-rings for gas bearing supported rotors," *Journal of Applied Mechanics*, Vol. 86, No. 8, p. 08100, Aug. 2019, https://doi.org/10.1115/1.4043473

[6] G. Belforte, F. Colombo, and T. Raparelli, "A theoretical study of a high speed rotor supported by air bearings monted on O-rings," in *International Conference on Tribology*, 2006.

[7] T. W. Giants and B. Viton, *O-Ring resilience study*. USA: El Segundo, 2001.

[8] J. M. Hill, "A review of partial solutions of finite elasticity and their applications," *International Journal of Non-Linear Mechanics*, Vol. 36, No. 3, pp. 447–463, May 2001, https://doi.org/10.1016/s0020-7462(00)00041-x

[9] P. Gardonio and S. J. Elliott, "Passive and active isolation of structural vibration transmission between two plates connected by a set of mounts," *Journal of Sound and Vibration*, Vol. 237, No. 3, pp. 483–511, Oct. 2000, https://doi.org/10.1006/jsvi.2000.3064

[10] L. Wang, Y. Li, and Z. L. Ma, "The radial stiffness calculation and parameter optimization of annular rubber shock absorber based on Mooney-Rivlin model," (in Chinese), *Acta Armamentarii*, Vol. 43, No. 1, pp. 35–45, 2022, https://doi.org/10.12382/bgxb.2022.a008

[11] L. Zhang, C. L. Xia, and L. Xun, "Finite element analysis of reciprocating seal ing component of radial single-piston pump," (in Chinese), *Machine Tool and Hydraulic*, Vol. 39, No. 5, pp. 101–104, 2011, https://doi.org/10.3969/j.issn.1001-3881.2011.05.034

[12] W. J. Guan, Q. G. Du, and P. Q. Liu, "Finite element analysis of the sealing performance of rubber O-ring," (in Chinese), *Lubrication Engineering*, Vol. 37, No. 6, pp. 60–64, 2012, https://doi.org/10.3969/j.issn.0254-0150.2012.06.014

[13] Q. Zhang, J. W. Shi, and S. F. Suo, "Finite element analysis of rubber materials based on Mooney-Rivlin models and Yeoh models," (in Chinese), *China Synthetic Rubber Industry*, Vol. 43, No. 6, pp. 468–471, 2020, https://doi.org/10.3969/j.issn.1000-1255.2020.06.006

[14] X. B. Li and Y. T. Wei, "An improved Yeoh constitutive model for hyperelasticmaterial," (in Chinese), *Engineering Mechanics*, Vol. 33, No. 12, pp. 8–43, 2016, https://doi.org/10.6052/j.issn.1000-4750.2015.05.0388

[15] M. J. Zheng, W. J. Wang, and Z. N. Chen, "Determination for mechanical constants of rubber Mooney-Rivlin model," (in Chinese), *China Rubber Industry*, Vol. 50, No. 8, pp. 462–465, 2003, https://doi.org/10.3969/j.issn.1000-890x.2003.08.003

[16] Y. S. Wang and Z. H. Nie, "Study on the correlation between stiffness and hardness of rubber parts based on Mooney-Rivlin model," (in Chinese), *Journal of Mechanical Strength*, Vol. 45, No. 3, pp. 692–700, 2023, https://doi.org/10.16579/j.issn.1001.9669.2023.03.026

[17] J. R. Luo, "Study on the performance degradation law of rubber isolation bearing under sea erosion environment," (in Chinese), Guangzhou University, Guangzhou, 2014.

[18] P. Q. Yin, "Measurements on stiffness and damping coefficients of "O" type rubber ring," (in Chinese), *Journal of Aerospace Power*, Vol. 8, No. 2, pp. 19–21, 1987.

[19] M. Y. Qi, T. An, and X. B. Xiao, "Calculation method and parameter optimization of resilient wheel stiffness considering nonlinear of rubber," (in Chinese), *Machinery Design and Manufacture*, Vol. 33, No. 2, pp. 206–210, 2023, https://doi.org/10.3969/j.issn.1001-3997.2023.02.042

[20] J. Chen, "Research on stiffness and damping characteristics of polyurethane rubber vibration absorber ring," (in Chinese), Nanjing University of Aeronautics and Astronautics, Nanjing, 2020.

[21] J. M. Horton, M. J. C. Gover, and G. E. Tupholme, "Stiffness of rubber bush mountings subjected to radial loading," *Rubber Chemistry and Technology*, Vol. 73, No. 2, pp. 253–264, May 2000, https://doi.org/10.5254/1.3547589

[22] J. M. Horton, M. J. C. Gover, and G. E. Tupholme, "Stiffness of rubber bush mountings subjected to tilting deflection," *Rubber Chemistry and Technology*, Vol. 73, No. 4, pp. 619–633, Sep. 2000, https://doi.org/10.5254/1.3547609

[23] L. S. Lin and Q. M. Chen, "Rubber hardness standard block and its temperature characteristics," (in Chinese), *Measurement Technique*, No. 8, pp. 32–35, 1994.

[24] K. Khaled and M. K. Singla, "Predictive analysis of groundwater resources using random forest regression," *Journal of Artificial Intelligence and Metaheuristics*, Vol. 9, No. 1, pp. 11–19, Jan. 2025, https://doi.org/10.54216/jaim.090102

[25] M. Mahmoud, "A review on waste management techniques for sustainable energy production," *Metaheuristic Optimization Review*, Vol. 3, No. 2, pp. 47–58, Jan. 2025, https://doi.org/10.54216/mor.030205

[26] E.-S. M. El-Kenawy, N. Khodadadi, S. Mirjalili, A. A. Abdelhamid, M. M. Eid, and A. Ibrahim, "Greylag Goose Optimization: nature-inspired optimization algorithm," *Expert Systems with Applications*, Vol. 238, No. 8, p. 122147, Mar. 2024, https://doi.org/10.1016/j.eswa.2023.122147

[27] G. Atteia et al., "Adaptive dynamic dipper throated optimization for feature selection in medical data," *Computers, Materials and Continua*, Vol. 75, No. 1, pp. 1883–1900, Jan. 2023, https://doi.org/10.32604/cmc.2023.031723

[28] P. Mishra et al., "Forecasting production of potato for a sustainable future: global market analysis," *Potato Research*, Vol. 67, No. 4, pp. 1671–1690, Mar. 2024, https://doi.org/10.1007/s11540-024-09717-0

Ting Deng is currently an engineer at the AECC Hunan Aviation Powerplant Research Institute. Master's degree. Her main research direction is rotor dynamics.

Xunyan Yin is currently a Lecturer at Shenyang University of Aeronautics and Astronautics. Doctor. Her main research direction is the strength and vibration of aircraft engines

Yuqi Yan is currently a graduate student in the School of Aero-engine, Shenyang Aerospace University, China. His major is energy and power, and his research interests include squeeze film damper and aero-engine vibration.

Hailun Zhou is currently an Professor in the School of Aero-engine, Shenyang Aerospace University, China. He received his Ph.D. in vehicle operation engineering from Nanjing University of Aeronautics and Astronautics. His research interests include squeeze film damper, rotor dynamic and aero-engine vibration.

Ran Zhang is currently a graduate student in the School of Aero-engine, Shenyang Aerospace University, China. His major is aeronautical and astronautical propulsion theory and engineering and his research interests include squeeze film damper and aero-engine vibration.

ISSN PRINT 1392-8716, ISSN ONLINE 2538-8460